[6] Donnell, L. H., "Stability of Thin-Walled Tubes under Torsion," Rept. 479, 1933, NASA.

[7] Chamis, C. C., "Micro and Structural Mechanics and Structural Synthesis of Multilayered Filamentary Composite Panels," DSMSD Rept. 9 under Contract No. AF 33(615)-3110, Sept. 1967, Case Western Reserve University, Cleveland, Ohio.

[8] Chao, T. L., "Minimum Weight Design of Stiffened Fiber Composite Cylinders," Ph.D. thesis, Sept. 1969, Case Western Reserve University, Cleveland, Ohio.

[9] Cheng, S. and Ho, B. P. C., "Stability of Heterogeneous Aeolotropic Cylindrical Shells under Combined Loading," *AIAA Journal*, Vol. 1, No. 4, April 1963, pp. 892–898.

[10] Kicher, T. P. and Mandell, J. F., "An Experimental Study of the Buckling of Anisotropic Plates," *AIAA/ASME 10th Structures, Structural Dynamics and Materials Conference, New Orleans, La.*, April 1969, pp. 380–385.

[11] Fiacco, A. V. and McCormick, G. P., "The Sequential Unconstrained Minimization Technique for Non-linear Programming, A Primal Dual Method," *Management Science*, Vol. 10, No. 2, Jan. 1964.

[12] Fletcher, R. and Powell, M. J. D., "A Rapidly Convergent Descent Method for Minimization," *Computer Journal (British)*, Vol. 6, 1963, pp. 163–168.

JULY 1971 J. AIRCRAFT VOL. 8, NO. 7

General Instability of Eccentrically Stiffened Cylindrical Panels

GEORGE J. SIMITSES*
Georgia Institute of Technology, Atlanta, Ga.

General instability of eccentrically stiffened thin cylindrical panels under the action of three types of applied loads is investigated. The three loads are uniform axial compression, uniform hoop compression or lateral pressure, and uniform shear. The analysis is based on a small-deflection theory for orthotropic shells which includes effects of stiffener eccentricity. Stiffener spacing is assumed to be sufficiently small (smeared technique), the stiffener geometry is taken to be uniform, and the skin-stiffener connection is assumed to be monolithic. The Galerkin procedure is employed to solve the buckling equations of the stiffened panels for the case of classical, simply supported boundaries. Critical loads were calculated from the resultant equations for two geometries: unstiffened isotropic panel and typical panel of the C-141 fuselage. Effects of stiffener eccentricity, panel aspect ratio, and the curvature parameter are shown in graphical form. When the initial curvature is set to zero, the results are applicable to flat rectangular simply supported plates. Finally, the C-5A Galaxy fuselage geometry was checked and shown to be safe for general instability failure.

Nomenclature

b	= width of curved plate (along nonzero curvature)
D_{xx},D_{yy},D_{xy}	= orthotropic flexural and twisting stiffnesses
e	= stringer and ring eccentricities
$\bar{e}$	= nondimensionalized eccentricities [$= \pi^2 Re/L^2$]
E_{xx},E_{yy}	= orthotropic extensional stiffnesses
G_{xy}	= in-plane skin shear stiffness
k_x,k_y,k_s	= applied load coefficients [see Eqs (3)]
L	= length of curves plate (along zero curvature)
m	= number of half-sine waves in x direction
M_x,M_y,M_{xy}	= moment resultants
n	= number of full-sine waves in y direction
N_x,N_y	= stress resultants
$\bar{N}_x,\bar{N}_y,N_{xy}{}^0$	= membrane stress resultants
q	= applied pressure (positive outward)
R	= cylindrical panel radius (to skin midsurface)
w	= normal displacement component (radial) of reference surface points
Z_t	= curvature parameter [$= \{(1-\nu^2)E_{xx}L^4/12R^2D_{yy}{}^{1/2}\}$]
α_{mn}	= [see Eq. (8)]
λ_{ij},ρ_{ij}	= extensional and flexural stiffness parameters [see Eq. (3)]
ν	= Poisson's ratio
p	= subscript referring to panel
r,st	= subscripts referring to ring and stringer, respectively

Received November 25, 1969; revision received August 18, 1970.

* Associate Professor of Engineering Science and Mechanics. Associate Fellow AIAA.

Introduction

GENERAL instability of eccentrically stiffened thin shells is one type of buckling and is defined as loss of stability in a mode in which all of the components of the stiffened shell (i.e., the stiffeners and skin) participate and the deformation extends over the entire surface of the shell. This type of buckling of eccentrically stiffened complete thin cylindrical shells has been extensively studied by many authors since the 1930's. (For a fairly complete bibliography, see Refs. 1 and 2.)

Since the complete cylinder results are not directly applicable to the stiffened partial cylindrical panel, general instability of such structural elements is investigated, with special attention to the effects of stiffener eccentricity, curvature, and panel aspect ratio, under the action of three types of applied loads. These three types of loads are uniform axial compression, uniform hoop compression or lateral pressure, and uniform shear.

Stability studies of curved cylindrical panels of isotropic geometry under pressure, shear, and axial compression have been reported by Rafel,[3,4] Rafel and Sandlin,[5] Schildcraut and Stein,[6] and Batdorf et al.[7,8] the effect of a single stiffening member on the stability of curved cylindrical panels has been reported by Stein and Yaeger[9] and Batdorf and Schildcrout.[10] For a more complete bibliography and a comprehensive discussion of these problems, see Refs. 11 and 12.

In the early 1950's, a theory was developed by Stein and Mayers[13] to analyze curved plates of sandwich construction. The same authors[14] used their theory to predict buckling of

simply supported curved plates of sandwich construction under uniform axial compression.

The present analysis is based on a small-deflection theory for orthotropic shells which includes effects of stiffener eccentricity. No results have been reported in the open literature for such geometric configurations. Since the isotropic geometry and the complete cylinder (stiffened or unstiffened) are special cases of the configuration under consideration, these geometries are used as check points for the present analysis.

Governing Equations

The nomenclature, geometry, and sign convention are the same as those of Ref. 15. The buckling equation [Eq. (4) of Ref. 15] is slightly different from that used in the present analysis. The difference is that in the present analysis it is assumed that the lateral pressure remains parallel to its original direction, whereas in Ref. 15 it is assumed that the pressure remains normal to the deflected midsurface during buckling.

Note that in this case, as in the case of a complete cylinder, it is assumed that a primary equilibrium state exists (the effect of prebuckling deformations is negligible) and the problem is reduced to a linear eigen-boundary-value problem.

On the basis of the preceding, the governing buckling equation is

$$\nabla_D w^1 + [12Z_t^2/\pi^4(1-\nu^2)]\nabla_E^{-1}\nabla_C w^1 = (L/\pi)^2[-k_x\rho_{xx}w_{,xx}{}^1 + k_y w_{,yy}{}^1 + 2k_s w_{,xy}{}^1] \quad (1)$$

where

$$\nabla_E = \left(\frac{L}{\pi}\right)^4\left[\frac{\partial^4}{\partial x^4} + \left(\frac{\lambda_{yy}}{\lambda_{xy}} - \nu\lambda_{xx_p} - \nu\lambda_{yy_p} - \nu^2\frac{\lambda_{xx_p}\lambda_{yy_p}}{\lambda_{xy}}\right)\frac{\partial^4}{\partial x^2\partial y^2} + \lambda_{yy}\frac{\partial^4}{\partial y^4}\right] \quad (2a)$$

$$\nabla_D = \left(\frac{L}{\pi}\right)^4\left[\rho_{xx}\frac{\partial^4}{\partial x^4} + 2\left(\rho_{xy} + \frac{\nu}{2}\rho_{xx_p} + \frac{\nu}{2}\rho_{yy_p}\right)\times\frac{\partial^4}{\partial x^2\partial y^2} + \frac{\partial^4}{\partial y^4}\right] \quad (2b)$$

$$\nabla_C = \left(\frac{L}{\pi}\right)^8\left[\bar{e}_x{}^2\lambda_{xx_{st}}\lambda_{xx_p}\frac{\partial^8}{\partial x^8} + \bar{e}_x{}^2\lambda_{xx_{st}}\left(\lambda_{xx_p}\frac{\lambda_{yy}}{\lambda_{xy}} - \nu\lambda_{xx_p} - \nu\lambda_{yy_p} - \nu^2\frac{\lambda_{xx_p}\lambda_{yy_p}}{\lambda_{xy}}\right)\frac{\partial^8}{\partial x^6\partial y^2} + \left\{\bar{e}_x{}^2\lambda_{xx_{st}}\lambda_{yy} + \bar{e}_x\bar{e}_y\lambda_{xx_{st}}\lambda_{yy_r}\left(2 + \nu\frac{\lambda_{xx_p} + \lambda_{yy_p}}{\lambda_{xy}}\right) + \bar{e}_y{}^2\lambda_{yy_r}\right\}\frac{\partial^8}{\partial x^4\partial y^4} + \bar{e}_y{}^2\lambda_{yy_r}\left(\frac{\lambda_{yy_p}}{\lambda_{xy}} - \nu\lambda_{xx_p} - \nu\lambda_{yy_p} - \nu^2\frac{\lambda_{xx_p}\lambda_{yy_p}}{\lambda_{xy}}\right)\frac{\partial^8}{\partial x^2\partial y^6} + \bar{e}_y{}^2\lambda_{yy_r}\lambda_{yy_p}\frac{\partial^8}{\partial y^8} + \nu\bar{e}_x\lambda_{xx_{st}}(\lambda_{xx_p} + \lambda_{yy_p})\left(\frac{\pi}{L}\right)^2\frac{\partial^6}{\partial x^6} - 2(\bar{e}_x\lambda_{xx_{st}}\lambda_{yy} + \bar{e}_y\lambda_{yy_r})\left(\frac{\pi}{L}\right)^2\frac{\partial^6}{\partial x^4\partial y^2} + \nu\bar{e}_y\lambda_{yy_r}(\lambda_{xx_p} + \lambda_{yy_p})\left(\frac{\pi}{L}\right)^2\frac{\partial^6}{\partial x^2\partial y^4} + (\lambda_{yy} - \nu^2\lambda_{xx_p}\lambda_{yy_p})\left(\frac{\pi}{L}\right)^4\frac{\partial^4}{\partial x^4}\right] \quad (2c)$$

$$Z_t^2 = (1-\nu^2)\frac{L^4E_{xx}}{12R^2D_{yy}} \qquad \bar{e} = \left(\frac{\pi R}{L}\right)^2\frac{e}{R}$$

$$\lambda_{ij} = \frac{E_{ij}\text{ or }G_{ij}}{E_{xx}}$$

$$\rho_{ij} = \frac{D_{ij}}{D_{yy}} \qquad k_x = \frac{\bar{N}_xL^2}{\pi^2D_{xx}} \qquad k_y = \frac{\bar{N}_y\bar{L}^2}{\pi^2D_{yy}} \quad (3)$$

$$k_s = \frac{N_{xy}{}^0L^2}{\pi^2D_{yy}} \qquad \lambda_{xx_{st}} + \lambda_{xx_p} = 1 \qquad \lambda_{yy_r} + \lambda_{yy_p} = \lambda_{yy}$$

The classical, simply supported boundary conditions are given by (note that the curved plate is L units long in the

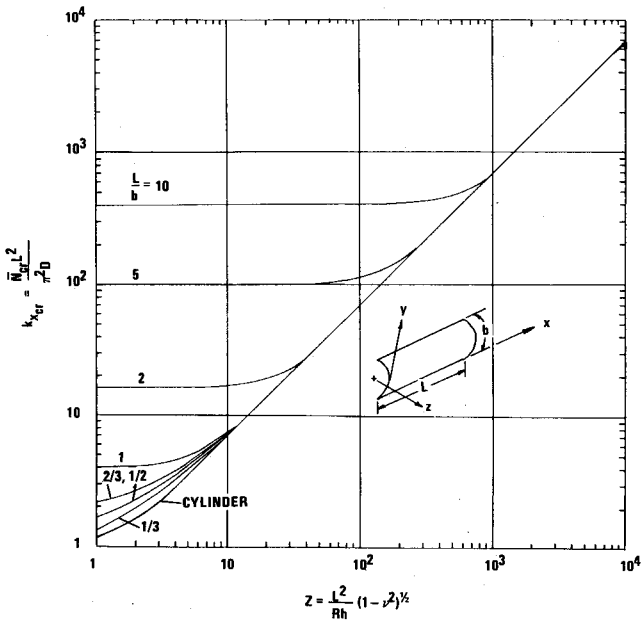

Fig. 1 Critical axial compression; effect of aspect ratio (isotropic).

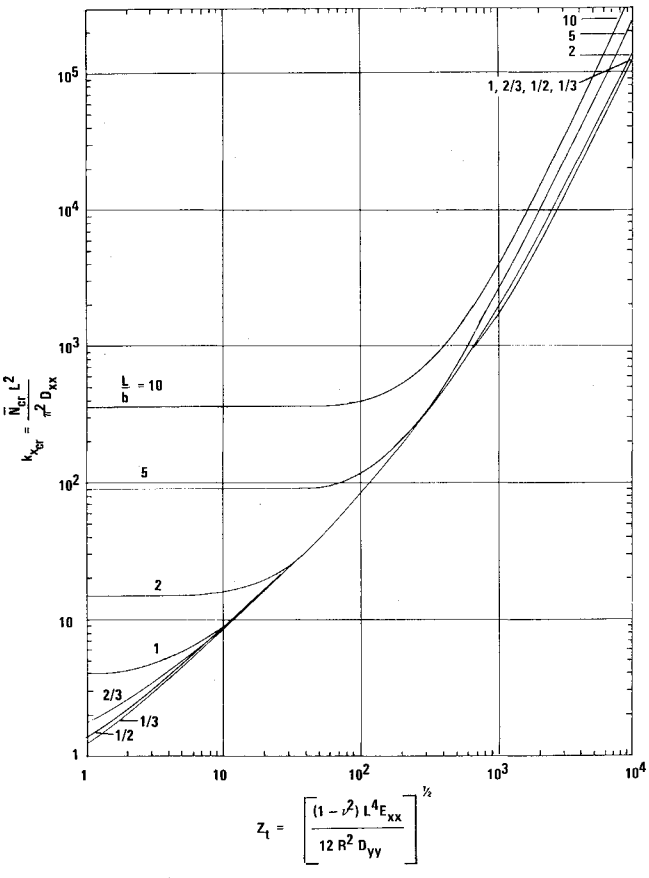

Fig. 2 Critical axial compression; effect of aspect ratio (stiffened).

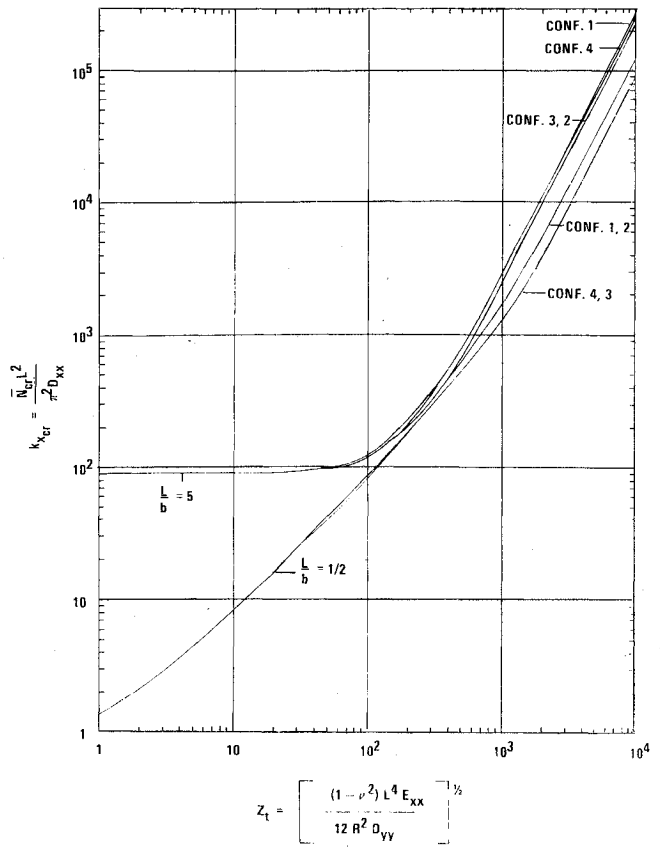

Fig. 3 Critical axial compression; effect of stiffener positioning.

x direction and b units long in the curved y direction)

$$\begin{aligned} w^1(0,y) &= w^1(L,y) = 0 & M_x{}^1(0,y) &= M_x{}^1(L,y) = 0 \\ w^1(x,0) &= w^1(x,b) = 0 & M_y{}^1(x,0) &= M_y{}^1(x,b) = 0 \\ N_x{}^1(0,y) &= N_x{}^1(L,y) = 0 & v^1(0,y) &= v^1(L,y) = 0 \\ N_y{}^1(x,0) &= N_y{}^1(x,b) = 0 & u^1(x,0) &= u^1(x,b) = 0 \end{aligned} \tag{4}$$

Making use of the linearized version of the constitutive and kinematic relations, the boundary conditions can be expressed solely in terms of the displacement functions u^1, v^1, w^1 and their derivatives. The final form of the boundary conditions is given by

$$\begin{aligned} & w^1(0,y) = w^1(L,y) = 0 \\ & -(D_{xx} + e_x{}^2E_{xx_{st}})w_{,xx}{}^1(0,y) + e_xE_{xx_{st}}u_{,x}{}^1(0,y) = 0 \\ & -(D_{xx} + e_x{}^2E_{xx_{st}})w_{,xx}{}^1(L,y) + e_xE_{xx_{st}}u_{,x}{}^1(L,y) = 0 \\ & w^1(x,0) = w^1(x,b) = 0 \\ & -(D_{yy} + e_y{}^2E_{yy_r})w_{,yy}{}^1(x,0) + e_yE_{yy_r}v_{,y}{}^1(x,0) = 0 \\ & -(D_{yy} + e_y{}^2E_{yy_r})w_{,yy}{}^1(x,b) + e_yE_{yy_r}v_{,y}{}^1(x,b) = 0 \\ & E_{xx}u_{,x}{}^1(0,y) - e_xE_{xx_{st}}w_{,xx}{}^1(0,y) = 0 \\ & E_{xx}u_{,x}{}^1(L,y) - e_xE_{xx_{st}}w_{,xx}{}^1(L,y) = 0 \\ & v^1(0,y) = v^1(L,y) = 0, \quad u^1(x,0) = u^1(x,b) = 0 \\ & E_{yy}v_{,y}{}^1(x,0) - e_yE_{yy_r}w_{,yy}{}^1(x,0) = 0 \\ & E_{yy}v_{,y}{}^1(x,b) - e_yE_{yy_r}w_{,yy}{}^1(x,b) = 0 \end{aligned} \tag{5}$$

Note that all of the preceding boundary conditions are satisfied by each term of the following series representation for w^1:

$$w^1(x,y) = \sum_{m=1}^{\infty}\sum_{n=1}^{\infty} A_{mn} \sin\frac{m\pi x}{L} \sin\frac{n\pi y}{b} \tag{6}$$

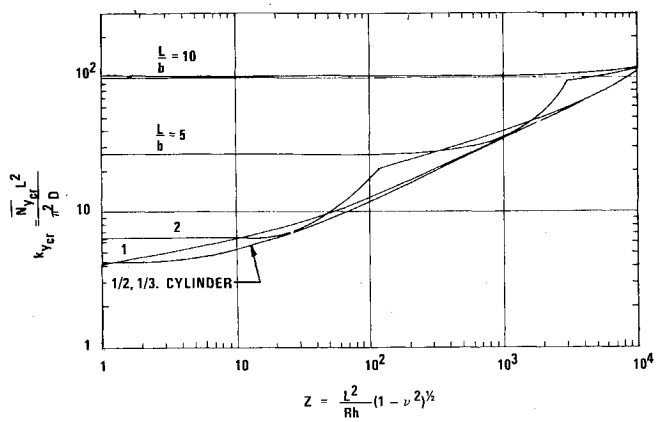

Fig. 4 Critical pressure or hoop compression; effect of aspect ratio (isotropic).

If the Galerkin procedure is employed and the indicated integrations are performed, the result is an infinite system of linear, homogeneous algebraic equations in A_{mn}, or

$$A_{mn}\alpha_{mn} + k_s \sum_{m'=1}^{\infty}\sum_{n'=1}^{\infty} A_{m'n'} \frac{mn\,m'n'}{(m'^2 - m^2)(n'^2 - n^2)} = 0$$

$$\text{for } m,n = 1,2,\ldots \tag{7}$$

where $m + m' = \text{odd}$, $n + n' = \text{odd}$, and where

$$\begin{aligned} \alpha_{mn} = \frac{\pi^2}{32}\left(\frac{b}{L}\right)\Bigg[& \rho_{xx}m^4 + 2\left(\rho_{xy} + \frac{\nu}{2}\rho_{xx_p} + \frac{\nu}{2}\rho_{yy_p}\right) \\ & \times m^2n^2\left(\frac{L}{b}\right)^2 + n^4\left(\frac{L}{b}\right)^4 + \Bigg[m^4 + \left(\frac{\lambda_{yy}}{\lambda_{xy}} - \right. \\ & \left.\nu\lambda_{xx_p} - \nu\lambda_{yy_p} - \nu^2\frac{\lambda_{xx_p}\lambda_{yy_p}}{\lambda_{xy}}\right)m^2n^2\left(\frac{L}{b}\right)^2 + \\ & \lambda_{yy}n^4\left(\frac{L}{b}\right)^4\Bigg]^{-1}\Bigg\{\frac{12Z_t{}^2}{\pi^4(1-\nu^2)}\Bigg[\bar{e}_x{}^2\lambda_{xx_{st}}\lambda_{xx_p}m^8 + \\ & \bar{e}_x{}^2\lambda_{xx_{st}}\left(\lambda_{xx_p}\frac{\lambda_{yy}}{\lambda_{xy}} - \nu\lambda_{xx_p} - \nu\lambda_{yy_p} - \right. \\ & \left.\nu^2\frac{\lambda_{xx_p}\lambda_{yy_p}}{\lambda_{xy}}\right)m^6n^2\left(\frac{L}{b}\right)^2 + \Bigg[\bar{e}_x{}^2\lambda_{xx_{st}}\lambda_{yy} + \\ & \bar{e}_x\bar{e}_y\lambda_{xx_{st}}\lambda_{yy_r}\left(2 + \nu\frac{\lambda_{xx_p} + \lambda_{yy_p}}{\lambda_{xy}}\right) + \\ & \bar{e}_y{}^2\lambda_{yy_r}\Bigg]m^4n^4\left(\frac{L}{b}\right)^4 + \bar{e}_y{}^2\lambda_{yy_r}\left(\frac{\lambda_{yy_p}}{\lambda_{xy}} - \nu\lambda_{xx_p} - \right. \\ & \left.\nu\lambda_{yy_p} - \nu^2\frac{\lambda_{xx_p}\lambda_{yy_p}}{\lambda_{xy}}\right)m^2n^6\left(\frac{L}{b}\right)^6 + \bar{e}_y{}^2\lambda_{yy_r}n^8\left(\frac{L}{b}\right)^8 - \\ & \nu\bar{e}_x\lambda_{xx_{st}}(\lambda_{xx_p} + \lambda_{yy_p})m^6 + 2(\bar{e}_x\lambda_{xx_{st}}\lambda_{yy} + \\ & \bar{e}_y\lambda_{yy_r})m^4n^2\left(\frac{L}{b}\right)^2 - \nu\bar{e}_y\lambda_{yy_r}(\lambda_{xx_p} + \lambda_{yy_p})m^2n^4\left(\frac{L}{b}\right)^4 + \\ & (\lambda_{yy} - \nu^2\lambda_{xx_p}\lambda_{yy_p})m^4\Bigg]\Bigg\} - k_x\rho_{xx}m^2 + k_yn^2\left(\frac{L}{b}\right)^2\Bigg] \end{aligned} \tag{8}$$

One should note that the system of equations given by Eqs. (7) can be decoupled into two systems, one corresponding to $m \pm n = \text{even}$ and one to $m \pm n = \text{odd}$. The former will be referred to as symmetric buckling ($m \pm n = \text{even}$) and is characterized by an even number of nodal lines and the antisymmetric by an odd number. Thus, in general, two characteristic equations are obtained, and both must be checked in predicting the critical condition for a given geometry.

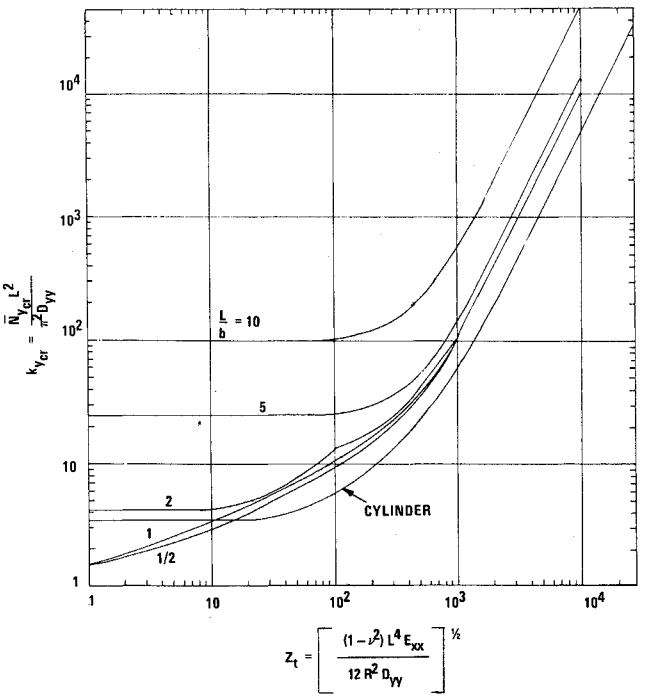

Fig. 5 Critical pressure or hoop compression; effect of aspect ratio (stiffened).

Note that, in the absence of shear ($k_s = 0$), the characteristic equation reduces to

$$\alpha_{mn} = 0 \tag{9}$$

If shear is present ($k_s \neq 0$), the characteristic equation is obtained by requiring a nontrivial solution to exist [for the system of Eqs. (7)]. This leads to the vanishing of the determinant of the coefficients of the A_{mn}'s.

Two typical determinants are shown below, one for symmetric buckling and one for antisymmetric. The size is kept to an 8×8 strictly for convenience:

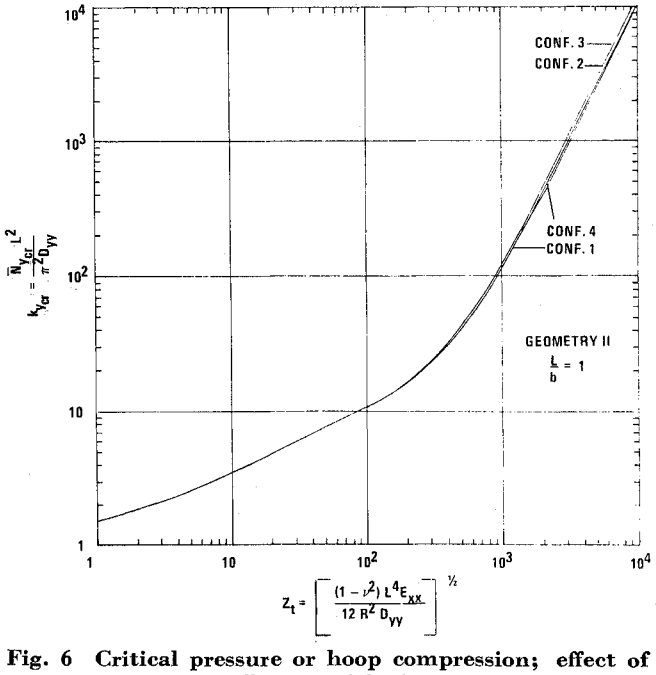

Fig. 6 Critical pressure or hoop compression; effect of stiffener positioning.

1) Symmetric, $(m \pm n)$ = even

m,n	A_{11}	A_{13}	A_{22}	A_{31}	A_{24}	A_{33}	A_{42}	A_{44}
1,1	$\frac{\alpha_{11}}{k_s}$	0	$\frac{4}{9}$	0	$\frac{8}{45}$	0	$\frac{8}{45}$	$\frac{16}{225}$
1,3	0	$\frac{\alpha_{13}}{k_s}$	$\frac{-4}{5}$	0	$\frac{8}{7}$	0	$\frac{-8}{25}$	$\frac{16}{35}$
2,2	$\frac{4}{9}$	$-\frac{4}{5}$	$\frac{\alpha_{22}}{k_s}$	$\frac{-4}{5}$	0	$\frac{36}{25}$	0	0
3,1	0	0	$\frac{-4}{5}$	$\frac{\alpha_{31}}{k_s}$	$\frac{-8}{25}$	0	$\frac{8}{7}$	$\frac{16}{35}$
2,4	$\frac{8}{45}$	$\frac{8}{7}$	0	$\frac{-8}{25}$	$\frac{\alpha_{24}}{k_s}$	$\frac{-72}{35}$	0	0
3,3	0	0	$\frac{36}{25}$	0	$\frac{-72}{35}$	$\frac{\alpha_{33}}{k_s}$	$\frac{-72}{35}$	$\frac{144}{49}$
4,2	$\frac{8}{45}$	$\frac{-8}{25}$	0	$\frac{8}{7}$	0	$\frac{-72}{35}$	$\frac{\alpha_{42}}{k_s}$	0
4,4	$\frac{16}{225}$	$\frac{16}{35}$	0	$\frac{16}{35}$	0	$\frac{144}{49}$	0	$\frac{\alpha_{44}}{k_s}$

$= 0$ (10)

2) Antisymmetric, $m \pm n$ = odd

m,n	A_{12}	A_{21}	A_{14}	A_{23}	A_{32}	A_{41}	A_{34}	A_{43}
1,2	$\frac{\alpha_{12}}{k_s}$	$\frac{-4}{9}$	0	$\frac{4}{5}$	0	$\frac{-8}{45}$	0	$\frac{8}{25}$
2,1	$\frac{-4}{9}$	$\frac{\alpha_{21}}{k_s}$	$\frac{-8}{45}$	0	$\frac{4}{5}$	0	$\frac{8}{25}$	0
1,4	0	$\frac{-8}{45}$	$\frac{\alpha_{14}}{k_s}$	$\frac{-8}{7}$	0	$\frac{-16}{225}$	0	$\frac{-16}{35}$
2,3	$\frac{4}{5}$	0	$\frac{-8}{7}$	$\frac{\alpha_{23}}{k_s}$	$\frac{-36}{25}$	0	$\frac{72}{35}$	0
3,2	0	$\frac{4}{5}$	0	$\frac{-36}{25}$	$\frac{\alpha_{32}}{k_s}$	$\frac{-8}{7}$	0	$\frac{72}{35}$
4,1	$\frac{-8}{45}$	0	$\frac{-16}{225}$	0	$\frac{-8}{7}$	$\frac{\alpha_{41}}{k_s}$	$\frac{-16}{35}$	0
3,4	0	$\frac{8}{25}$	0	$\frac{72}{35}$	0	$\frac{-16}{35}$	$\frac{\alpha_{34}}{k_s}$	$\frac{-144}{49}$
4,3	$\frac{8}{25}$	0	$\frac{-16}{35}$	0	$\frac{72}{35}$	0	$\frac{-144}{49}$	$\frac{\alpha_{43}}{k_s}$

$= 0$ (11)

The following load cases are considered for each geometry: 1) uniform axial compression (k_x); 2) uniform lateral pressure or uniform hoop compression (k_y); and 3) uniform shear (k_s). The characteristic equation for load cases 1 and 2 is given by Eq. (9), whereas for case 3 it is given by Eqs. (10) and (11).

A computer program was written, and numerical results are reported for two geometries: isotropic and typical C-141 fuselage geometry.

The isotropic geometry is characterized by the following values of the parameters:

$$\lambda_{xx_p} = \lambda_{yy_p} = \lambda_{yy} = 1$$

$$\lambda_{xx_{st}} = \lambda_{yy_r} = 0 \qquad \lambda_{xy} = \tfrac{1}{2}(1 - \nu)$$

$$\rho_{xx} = \rho_{xx_p} = \rho_{yy_p} = 1 \qquad \rho_{xy} = 1 - \nu$$

$$\bar{e}_x = \bar{e}_y = 0 \qquad Z_t = (L^2/Rh)(1 - \nu^2)^{1/2}$$

$$k_x = \bar{\sigma}_x h L^2/\pi^2 D = \bar{N}_x L^2/\pi^2 D$$

$$k_y = qRL^2/\pi^2 D = \bar{N}_y L^2/\pi^2 D$$

$$k_s = \tau_{xy} h L^2/\pi^2 D = \bar{N}_{xy} L^2/\pi^2 D \qquad \text{where}$$

$$D = Eh^3/12(1 - \nu^2)$$

The isotropic geometry is denoted by "Geometry I."

The typical C-141 fuselage geometry is denoted by "Geometry II," and it represents the fuselage geometry immediately aft of the rear landing gear frame of the C-141 Starlifter. This geometry is circular and is characterized by

$R = 85$ in. $\quad A_r = 0.248$ in.^{2} $\quad A_{st} = 0.260$ in.^{2}

$h = 0.05$ in. $\quad e_y = 1.585$ in. $\quad e_x = 0.310$ in.

$I_{x_c} = 0.034$ in.^{4} $\quad I_{y_c} = 0.309$ in.^{4} $\quad 1_x = 6$ in.

$1_y = 20$ in.

The parameters used in the analysis are computed on the basis of the preceding data, and they are

$\lambda_{xx_p} = 0.56 \quad \lambda_{yy_p} = 0.56 \quad \lambda_{yy} = 0.69$

$\lambda_{xx_{st}} = 0.44 \quad \lambda_{yy_r} = 0.13 \quad \lambda_{xy} = 0.20$

$\rho_{xx_p} \simeq \rho_{yy_p} \simeq 0 \quad \rho_{xx} = 0.367 \quad \rho_{xy} = 0.050$

$\bar{e}_x = \pm\ (0.003647) \quad \bar{e}_y = \pm\ (0.018647)$

where the positive sign is associated with external positioning of the stiffeners, and the negative sign with internal positioning.

Discussion of Results

A computer program was written, and critical loads are obtained for both geometries. Parametric studies are made by varying the following parameters:

1) $L/b = \frac{1}{3}, \frac{1}{2}, \frac{2}{3}, 1, 2, 5, 10$.

2) $Z_t = 0, 1, 10, 30, 100, 300, 1000, 3000$ and 10,000.

3) All four combinations of stiffener positioning are considered: configuration 1, stringers in, rings out $(-,+)$; configuration 2, stringers in, rings in $(-,-)$; configuration 3, stringers out, rings in $(+,-)$; and configuration 4, stringers out, rings out $(+,+)$.

Through this, the effect of stiffener positioning is studied (for Geometry II). The generated data are presented in graphical form (in part; see Figs. 1–9), and the results are discussed individually for each load case. The conclusions concerning eccentricity effects should not be generalized, since they were drawn on the basis of the geometry used.

1. Axial Compression

The characteristic equation is given by Eq. (9). This equation is first solved for k_x by setting k_y equal to zero, and critical values for k_x are obtained through minimizations with respect to integer values of m and n. Values of $k_{x_{cr}}$ are plotted vs the curvature parameter Z_t in Figs. 1–3.

In Fig. 1, the results for the isotropic geometry (Geometry I) are presented. These results are in excellent agreement with those of previous investigations.[6,14] The complete cylinder results[14] appear as a lower bound, and the effect of aspect ratio L/b is concentrated on the lower end of Z values. For a given curvature parameter Z and length L, the critical load increases as the aspect ratio L/b increases.

The results corresponding to the stiffened geometry (Geometry II) are presented in Figs. 2 and 3. In Fig. 2, the effect of aspect ratio is presented for configuration 2. This effect is the same for all other configurations and very similar to that of the isotropic geometry. The eccentricity effect for $L/b = 2$, 5, and 10 is similar to that corresponding to the complete cylinder. For these aspect ratios, the weakest configuration corresponds to having the rings on the inside and the strongest to having the rings on the outside for all values of Z_t. As far as stringers are concerned, certain reversals take place. At the lower values of Z_t, inside stringers yield a weaker configuration than outside stringers. At the higher values of Z_t ($Z_t > 100$), this effect is reversed. Thus, for low values of Z_t ($Z_t \leq 100$), the order in going from the weakest to the strongest configuration is 2, 3, 1, 4, whereas for large values of Z_t ($Z_t > 100$), this order becomes 3, 2, 4, 1 (see Fig. 3). Please note that the difference in critical values at the lower range of Z_t is very small.

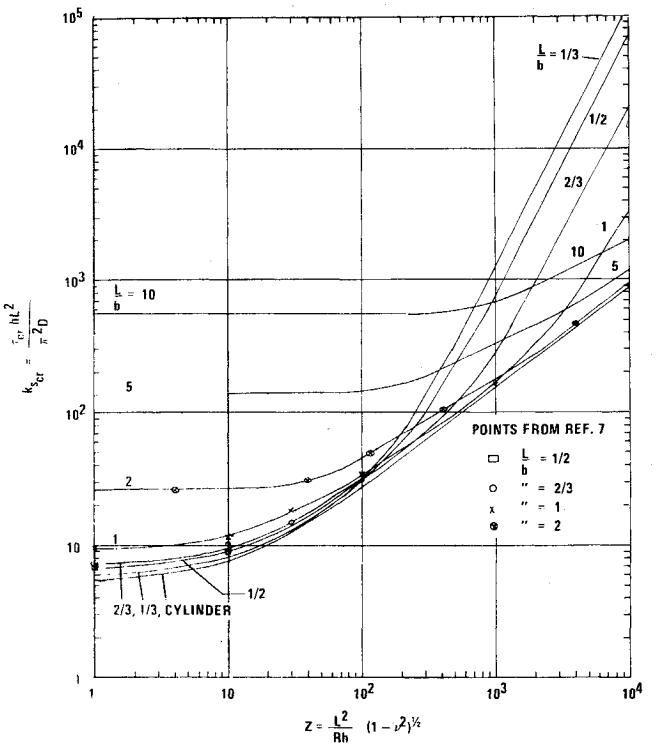

Fig. 7 Critical shear; effect of aspect ratio (isotropic).

2. Pressure or Hoop Compression

This load case corresponds to either a pressure loading, in which case $k_{y_{cr}}$ is an index of critical pressure, or to a hoop

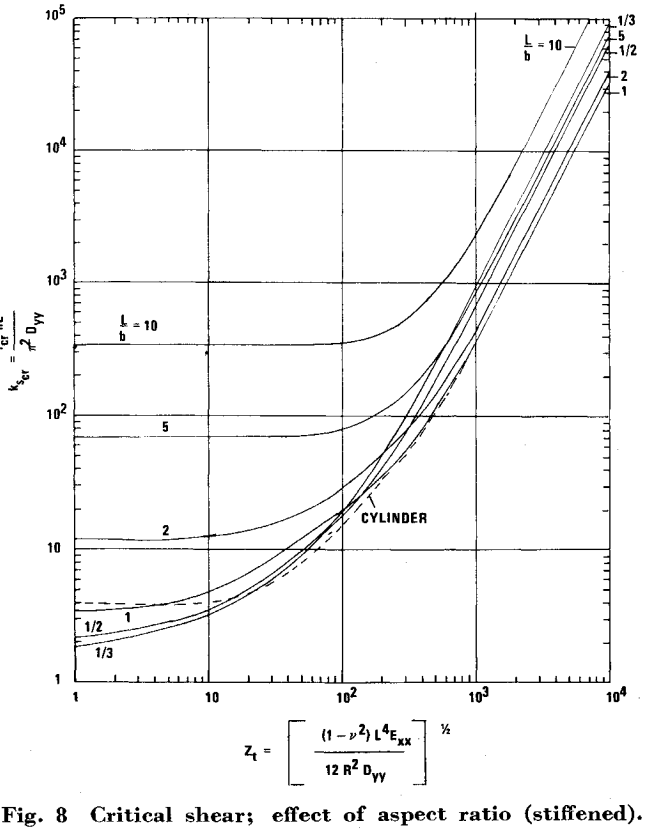

Fig. 8 Critical shear; effect of aspect ratio (stiffened).

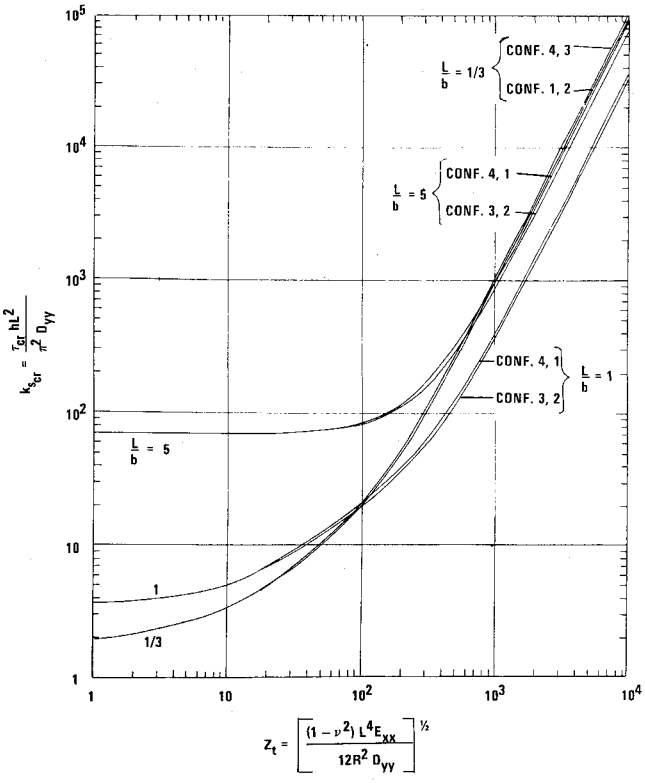

Fig. 9 Critical shear; effect of stiffener positioning.

compression, in which case $k_{y_{cr}}$ is an index of critical compression in the hoop direction. Note that for both of these cases it has been assumed that a primary state exists, and therefore the geometry remains cylindrical up to the instant of buckling.

The characteristic equation is also given by Eq. (9), and critical loads are obtained by first setting $k_x = 0$ and then minimizing k_y with respect to integer values of m and n. Values of $k_{y_{cr}}$ are plotted vs the curvature parameter Z_t in Figs. 4–6.

In Fig. 4, the results corresponding to the isotropic geometry are presented. These results are in excellent agreement with the flat plate classical results (see Ref. 16, compression in the y direction) and do reduce to the high circular arch result[16] when the panel is taken to be very long.

The effect of aspect ratio L/b is similar to that for k_x, with the exception that for $L/b \geq 1$ the curves cross each other for a small range of Z_t values. The curve corresponding to the complete cylinder appears to be a lower bound for this case also.

The results corresponding to the stiffened geometry are presented in Figs. 5 and 6. In Fig. 5, the effect of aspect ratio L/b is presented for configuration 1, which is the weakest configuration for the entire range of Z_t values considered. The effect of aspect ratio is the greatest at the lower values of Z_t, and it decreases with increasing Z_t. This effect is the same for all four configurations. In this case also, the curve corresponding to the complete cylinder appears to be a lower bound for all values of Z_t except $Z_t < 15$ (see Fig. 5). For this load case, the eccentricity effect is the same as for the complete cylinder for all values of the aspect ratio L/b. Furthermore, the order in going from the weakest to the strongest configuration is independent of the value of the curvature parameter. This order is 1, 4, 2, 3.

Note that, when k_y represents the case of pressure loading, the present results correspond to the case where the loading is assumed to remain parallel to its original direction during buckling. It has been shown for complete cylinders[17] that the effect of load behavior, during the buckling process, becomes important as the cylinder length becomes very large.

3. Uniform Shear

The characteristic equation for this case is given by either Eq. (10) or Eq. (11) (not necessarily limited to an 8×8 determinant). A program was written such that, when $L/b < \frac{1}{2}$, $m = 1$ through 5 and $n = 1$ through 9 for the symmetric case and antisymmetric cases. Thus the size of the determinant for the symmetric case is 23×23, whereas the size of the determinant for the antisymmetric case is 22×22. Similarly, for $\frac{1}{2} < L/b < 2$, $m = 1$ through 7 and $n = 1$ through 7, which resulted in a 25×25 determinant for the symmetric case, and a 24×24 for the antisymmetric case. Finally, when $L/b > 2$, $m = 1$ through 9 and $m = 1$ through 5. This was done in order to keep the size of the determinant of the same order of magnitude and have sufficient modal representation along both directions regardless of the L/b ratio. Numerical results were generated for both geometries, and part of these data are presented graphically in Figs. 7–9.

In Fig. 7, the results corresponding to the isotropic geometry are presented. On the same figure, data taken from Ref. 7 (Table 2) are shown for comparison. Two important observations are made based on the generated data. First, the curve corresponding to the complete cylinder appears to be a lower bound for the critical shear throughout the range of Z values and for all values of the aspect ratio. Second, for a given value of Z and a given length, there seems to be an aspect ratio that corresponds to the weakest configuration. This value of L/b is a function of the curvature parameter. Note from Fig. 7 that for $Z \leq 80$ the weakest configuration corresponds to $L/b = \frac{1}{3}$. As Z increases, the weakest configuration changes to $L/b = \frac{1}{2}$ ($80 < Z < 130$), to $\frac{2}{3}$ ($130 < Z_t < 300$), etc. For $1250 < Z < 10{,}000$, the weakest configuration corresponds to $L/b = 2$.

In comparing the present results with those of Ref. 7, it is observed that the agreement for $L/b = \frac{1}{2}, \frac{2}{3}$, 1, and 2 is excellent (calculated data taken from Table 2 of Ref. 7). Furthermore, the curves shown on Fig. 1 of Ref. 7 agree with the present results. The difference is that in Ref. 7 very limited data were generated, and the reader, when studying this Fig. 1 of Ref. 7, is under the impression that the complete cylinder results and the results corresponding to $L/b = 1$ represent the lower and upper bounds, respectively. This is not so, and the curve crossings are not shown (see Fig. 7). At this point, the reader should be cautioned as to the validity of the results for large values of the curvature parameter. As the curvature parameter increases, in general, the wavelengths decrease, and harmonics higher than those considered are needed to represent the buckled form sufficiently. In this case, a larger size determinant must be used.

In Fig. 8, the effect of aspect ratio is shown for configuration 2 of the stiffened geometry. This effect is the same for all other configurations. Configuration 2 (both stiffeners on the inside) represents the weakest configuration for the entire range of Z_t values. This effect is the same as for the isotropic geometry. These curves do cross over, and for $Z_t < 70$ the critical shear corresponding to $L/b = \frac{1}{3}$ is the smallest. As Z_t increases, changes take place, and for $Z_t > 200$ the critical shear corresponding to $L/b = 1$ is the smallest. Furthermore, the curve corresponding to the complete cylinder is a lower bound for $Z_t > 30$.

The effect of stiffener positioning is shown in Fig. 9. From the generated data, the following observations may be reported for the stiffened geometry. For the lower values of Z_t, the effect of stiffened positioning is identical to that of the complete cylinder.[1] For the complete cylinder, inside rings yield a weaker configuration than outside rings (primary effect). Furthermore, inside stiffeners have a weakening effect. Thus, in going from the weakest to the strongest configuration, one may write 2, 3, 1, 4. At the higher values

of Z_t, the effect of stiffener positioning for the panel deviates from that for the cylinder. The primary effect is the positioning of the stringers rather than rings. Thus, the order in going from the weakest to the strongest configuration becomes 2, 1, 3, 4. The value of Z_t at which the just-described reversal takes place depends on the aspect ratio. The lower range in which the cylinder behavior is noticed increases with increasing L/b values, to the point that at $L/b = 5$ and 10 the entire Z_t range considered belongs in the cylinder behavior range. This means that, for $L/b = 5$ and 10 and $0 < Z_t < 10{,}000$, the order in going from the weakest to the strongest configuration is 2, 3, 1, 4.

General Instability Loads for the C-5A Fuselage

The present program was used to predict the general instability loads for the C-5A Galaxie fuselage side panels. Three configurations were used which are typical for different fuselage stations. Because the stringer spacing varies from 20 to 35 in., four values for l_r were considered: $l_r = 20$, 25, 30, and 35 in. In addition, the length of the panel was considered to be $2R$, $3R$, and $4R$. The common data, for all three configurations, that characterize the C-5A geometry are

$R = 143$ in. $\quad A_r = 1.4$ in.^{2} $\quad I_{y_c} = 10$ in.^{4} $\quad e_y = -3$ in.

$l_x = 7.8$ in. $\quad b = 176$ in. $\quad E = 10^7$ psi $\quad \nu = 0.3$

The data that characterize the three configurations are as follows: configuration A, $A_x = 0.26$ in.^{2}, $I_{x_c} = 0.06$ in.^{4}, $h = 0.125$ in., $e_x = -1.17$ in.; configuration B, $A_x = 0.25$ in.^{2}, $I_{x_c} = .06$ in.^{4}, $h = 0.100$ in., $e_x = -1.15$ in.; and configuration C, $A_x = 0.18$ in.^{2}, $I_{x_c} = 0.041$ in.^{4}, $h = 0.085$ in., $e_x = -1.21$ in.

From the computed loads, it was found that the smallest compressive critical stress is 88,820 psi, corresponding to configuration A, $l_r = 35$ in., and it is independent of the L/R ratio. The smallest critical pressure is 21.73 psi, corresponding to configuration C, $l_r = 35$ in., and $L/R = 4$. Finally, the smallest critical shear stress is 118,800 psi, corresponding to configuration A, $l_r = 35$ in., and $L/R = 3$. Since the critical stresses are much greater than the ultimate stresses (in shear and compression) of the material used, it is concluded that the C-5A Galaxy geometry is not critical for general instability failure.

References

[1] Simitses, G. J., "Buckling of Eccentrically Stiffened Cylinders under Torsion," *AIAA Journal*, Vol. 6, No. 10, Oct. 1968, pp. 1856–1860.

[2] Singer, J. and Baruch, M., "Recent Studies on Optimization for Elastic Stability of Cylindrical and Conical Shells," *The Fifth Congress of the International Council of the Aeronautical Sciences*, London, Sept. 1966, Paper 66-13.

[3] Rafel, N., "Effect of Normal Pressure on the Critical Compressive Stress of Curved Sheet," WR L-258, 1942, NACA.

[4] Rafel, N., "Effect of Normal Pressure on the Critical Shear Stress of Curved Sheet," WR L-416, 1943, NACA.

[5] Rafel, N. and Sandlin, C. W., Jr., "Effect of Normal Pressure on the Critical Compressive and Shear Stress of Curved Sheet," WR L-57, 1944, NACA.

[6] Schildcrout, M. and Stein, M., "Critical Combination of Shear and Direct Axial Stress for Curved Rectangular Panels," TN 1928, 1949, NACA.

[7] Batdorf, S. B. et al., "Critical Shear Stress of Curved Rectangular Panels," TN 1348, 1947, NACA.

[8] Batdorf, S. B. et al. "Critical Combinations of Shear and Longitudinal Direct Stress for Long Plates with Transverse Curvature," TN 1347, 1947, NACA.

[9] Stein, M. and Yaeger, D. J., "Critical Shear Stress of a Curved Rectangular Panel with a Central Stiffener," TN 1972, 1949, NACA.

[10] Batdorf, S. B. and Schnildcrout, M., "Critical Axial-Compressive Stress of a Curved Rectangular Panel with a Central Chordivise Stiffener," TN 1661, 1948, NACA.

[11] Gerard, G. and Becker, H., "Handbook of Structural Stability. Part III—Buckling of Curved Plates and Shells," TN 3783, 1957, NACA.

[12] Becker, H., "Handbook of Structural Stability. Part VI—Strength of Stiffened Curved Plates and Shells," TN 3786, 1958, NACA.

[13] Stein, M. and Mayers, J., "A Small-Deflection Theory of Curved Sandwich Plates," TR 1008, 1951, NACA.

[14] Stein, M. and Mayers, J., "Compressive Buckling of Simply Supported Curved Plates and Cylinders of Sandwich Construction," TN 2601, 1952, NACA.

[15] Simitses, G. J., "A Note on the General Instability of Eccentrically Stiffened Cylinders," *Journal of Aircraft*, Vol. 4, No. 5, May 1967, pp. 473–475.

[16] Timoshenko, S. P. and Gere, J. M., *Theory of Elastic Stability*, McGraw-Hill, New York, 1959.

[17] Simitses, G. J., "Buckling of Eccentrically Stiffened Cylinders under Combined Loads," *AIAA Journal*, Vol. 7, No. 2, Feb. 1969, pp. 335–337.